The effects of oscillatory feeding of CO and O2 on the performance of a monolithic catalytic converter of automobile exhaust gas : a modelling study

The effects of oscillatory feeding of CO and O_2 on the performance of a monolithic catalytic converter of automobile exhaust gas: a modelling study

A.B.K. Lie, J. Hoebink and G.B. Marin

Laboratorium voor Chemische Technologie, Eindhoven University of Technology, PO Box 513, NL-5600 MB Eindhoven (Netherlands)

(Received January 4, 1993; in final form April 30, 1993)

Abstract

A monolithic catalytic converter of automobile exhaust gas was modelled in order to assess the effects of oscillatory feeding on the performance of the reactor with respect to CO oxidation by O_2. Simulations were performed with an oscillating feed composition of CO and O_2. The influence of frequency, amplitude, phase angle and ratio of reactants in the feed on the time average CO conversion was investigated. An improvement relative to the steady state conversion of 10% maximum is obtained at temperatures below the light-off temperature, at frequencies below 0.1 Hz and an amplitude of 15%. The reverse effect is obtained from temperatures slightly above the light-off temperature upwards. These effects are strongest when CO and O_2 oscillate in counterphase. The explanation for this effect is given in terms of strongly changing surface coverage during cycling of the feed concentrations.

1. Introduction

The removal of harmful components from car exhaust gases is one of the main environmental concerns today. Most often one applies a so-called three-way catalyst [1, 2] which is located in the exhaust pipe of a car. The reactor is usually a monolith [3], *i.e.* a block of ceramic material with several thousand parallel channels which are coated with a washcoat. The washcoat consists of platinum, rhodium and ceria on an alumina support. These components catalyse the oxidation of CO and unburnt hydrocarbons to CO_2 and H_2O as well as the reduction of NO_x to N_2.

In order to allow both the oxidation and the reduction to take place to a large extent, the reactants have to be present in close-to-stoichiometric amounts. This is achieved by a so-called lambda sensor [1, 2] which measures the oxygen concentration in the exhaust gas. The signal of the sensor is sent to a microprocessor which compares the oxygen concentration with its setpoint and adjusts the amount of fuel injected into the engine. By this feedback the air-to-fuel ratio is kept within narrow limits around the value of 14.6 kilograms of air per kilogram of fuel, which is the desired so-called stoichiometric ratio for most commercially used fuels.

One of the consequences of the feedback control is that the concentrations of CO, NO_x, O_2 and hydrocarbons oscillate around their setpoints, in particular because of the time delay of the lambda sensor. The oscillations typically have an amplitude between 5 and 15% of the time average concentrations and a frequency between 0.5 and 3 Hz [4]. It has been found experimentally that under some circumstances oscillatory feeding of a catalytic chemical reactor may result in an increase of the time average conversion [5–9], especially in the case of automobile exhaust gas treatment [4, 10–14]. Cho [12] has shown experimentally that oscillations improve the exhaust gas converter's performance below its light-off temperature, while the air–fuel ratio should be close to the stoichiometric ratio above the light-off temperature.

Dynamic modelling studies have been performed by Cho [15], who considered a single catalyst pellet, and by Graham and Lynch [16] in a study on the kinetics of CO oxidation using a fixed bed recycle reactor.

In this study a monolithic catalytic converter was modelled to determine the effect of oscillating feed

0923-0467/93/$6.00

concentrations, also called cycling of the feed, on the time average conversions. Only CO oxidation was considered, because reported values of kinetic parameters are mostly limited to this reaction [17–20].

2. Model equations

2.1. Assumptions

For the development of the mathematical model several assumptions were made. The heat conductivity in the solid phase was not taken into account, since there exists sufficient evidence [21–24] that such an effect is relevant only for studies of light-off or hot spot behaviour. Temperature oscillations could be neglected because of the small amplitudes at a time average concentration level which is low in itself. The adiabatic temperature rise was calculated as 30 K. Nevertheless, the converter was modelled as an isothermal reactor in order to focus on the effects of oscillating feeds at a given temperature. The mass flow rates were assumed to be identical through each channel of the monolith, while in fact the radial velocity profile in the exhaust pipe causes the mass flow in the outer channels to be lower than in the inner channels [25, 26]. The flow in the channels is laminar, since the Reynolds number is typically between 50 and 250. Entrance effects were neglected, because the hydrodynamic entrance length is only a small fraction of the total length of the converter [21, 27]. Radial variations in concentration and velocity in the channels can be dealt with by applying the concept of the asymptotic value of the Sherwood number $Sh = 3.66$ for fully developed laminar flow in a circular channel with constant wall temperature [28]. The asymptotic value allows description of the mass transfer from bulk gas to washcoat by a mass transfer coefficient if the Graetz number is larger than 0.1, which is the case here. Diffusion coefficients were calculated using the method of Fuller *et al.* [29]. Pore diffusion limitation was neglected, since the washcoat thickness is typically around 25 μm. The Weisz–Prater criterion [30] was calculated to be 0.13 based on a rate of 20 mol m_{cat}^{-3} s^{-1}, a diffusivity of 10^{-6} m^2 s^{-1} and a gas concentration near the catalyst surface of 0.1 mol m^{-3}.

2.2. Rate equations

Most of the published kinetic studies of CO oxidation were carried out at lower temperatures than the actual working conditions of the commercial converter. As a consequence there are no suitable kinetic models which describe the temperature-dependent behaviour of the reaction over a wide temperature range. The kinetics of CO oxidation on the $Pt–Al_2O_3$ catalyst used in the present work were based on the kinetic study of Herz and Marin [19], which assumes the following elementary steps:

$$CO + * \underset{k_{d,1}}{\overset{k_{a,1}}{\rightleftharpoons}} CO* \quad (1)$$

$$O_2 + 2* \xrightarrow{k_{a,2}} 2O* \quad (2)$$

$$CO* + O* \xrightarrow{k_r} CO_2 + 2* \quad (3)$$

where * stands for a catalytic site.

The rate of adsorption of CO is described by

$$r_{a,1} = k_{a,1} C_{s,CO} L_t (1 - \theta_{CO*} - \theta_{O*}) \quad (4)$$

where θ_i is the fraction of catalytic sites covered with species i. The rate of desorption of CO is described by

$$r_{d,1} = k_{d,1} L_t \theta_{CO*} \quad (5)$$

The rate coefficients are given by

$$k_{a,1} = \left(\frac{RT_s}{2\pi M_{CO}}\right)^{1/2} L_t^{-1} S_{CO*} \quad (6)$$

$$k_{d,1} = A_{d,1} \exp\left(-\frac{E_{A,d,1}}{RT_s}\right) \quad (7)$$

Note that $(RT_s/2\pi M_{CO})^{1/2}$ follows from the kinetic gas theory in units of m_f^3 m_{Pt}^{-2} s^{-1}. In contrast with Herz and Marin [19], the activation energy for desorption was considered to be independent of θ_{CO*}.

The adsorption of oxygen was assumed to be irreversible and dissociative and described by the rate equation [19]

$$r_{a,2} = k_{a,2} C_{s,O_2} L_t \left(1 - \frac{1-2\theta_O}{1-\theta_O}\theta_{CO*} - 2\theta_{O*}\right)^2 \quad (8)$$

with the adsorption rate coefficient given by

$$k_{a,2} = \left(\frac{RT_s}{2\pi M_{O_2}}\right)^{1/2} L_t^{-1} S_{O*} \quad (9)$$

and the sticking coefficient by

$$S_{O*} = S_{O_2} A_{a,2} \exp\left(-\frac{E_{A,a,2}}{RT_s}\right) \quad (10)$$

The rate of the surface reaction between the adsorbed species follows from

$$r = k_r L_t \theta_{CO} \theta_O \quad (11)$$

with the rate coefficient

$$k_r = A_r \exp\left(-\frac{E_{A,r}}{RT_s}\right) \quad (12)$$

TABLE 1. Kinetic parameter values used in this study

Parameter	Value
S_{CO*}	0.5
$A_{d,1}$	6.72×10^{14} s^{-1}
$E_{A,d,1}$	124.0 kJ mol^{-1}
S_{O_2}	1.0
$A_{a,2}$	4.04×10^{-3}
$E_{A,a,2}$	-4.2 kJ mol^{-1}
A_r	2.0×10^{12} s^{-1}
$E_{A,r}$	125.0 kJ mol^{-1}
L_t	2.48×10^{-5} mol m$_{Pt}^{-2}$

Table 1 lists the kinetic parameter values used in the present study. Except for the Arrhenius parameters of the surface reaction, they are identical to those reported by Herz and Marin [19]. With these parameter values the calculated steady state reaction rates and temperature dependences are comparable with those obtained by Voltz *et al.* [17] under typical exhaust gas conditions. Also, phenomena such as hysteresis and multiplicity of steady states were not encountered.

2.3. Reactor model

The reactor model consists of a set of continuity equations for the reactants in the three phases considered: the gas phase, the pores of the washcoat and the catalyst surface. Since Bos and Westerterp [31] showed that neglecting density variations in tubular reactors may cause large errors, the dependent variables were expressed as C/ρ_f, *i.e.* in units of mol kg^{-1}.

The continuity equation for reactant i in the gas phase is given by

$$\epsilon\rho_f \frac{\partial}{\partial t}\left(\frac{C_{f,i}}{\rho_f}\right) = -\phi_m^{sup}\frac{\partial}{\partial x}\left(\frac{C_{f,i}}{\rho_f}\right) - k_f a_v (C_{f,i} - C_{s,i}) \tag{13}$$

which holds for both CO ($i=1$) and O_2 ($i=2$).

The continuity equation for CO ($i=1$) in the pores of the washcoat is given by

$$\epsilon_w\rho_f \frac{4\epsilon d_w}{d_b}\frac{\partial}{\partial t}\left(\frac{C_{s,1}}{\rho_f}\right) = k_f a_v (C_{f,1} - C_{s,1}) - a_{cat} r_{a,1} + a_{cat} r_{d,1} \tag{14}$$

and for O_2 ($i=2$) by

$$\epsilon_w\rho_f \frac{4\epsilon d_w}{d_b}\frac{\partial}{\partial t}\left(\frac{C_{s,2}}{\rho_f}\right) = k_f a_v (C_{f,2} - C_{s,2}) - a_{cat} r_{a,2} \tag{15}$$

The continuity equations for CO* and O* on the surface of the catalyst are given by

$$\frac{\partial\theta_{CO*}}{\partial t} = (r_{a,1} - r_{d,1} - r)\frac{1}{L_t} \tag{16}$$

$$\frac{\partial\theta_{O*}}{\partial t} = (2r_{a,2} - r)\frac{1}{L_t} \tag{17}$$

The reactor is assumed to operate under steady state conditions before starting any oscillation of the feed. Hence the initial conditions are

$$C_{f,i}(x, 0) = C_{f,i}(x)^{ss}, \quad 0 \leqslant x \leqslant L \tag{18}$$

$$C_{s,i}(x, 0) = C_{s,i}(x, 0)^{ss}, \quad 0 \leqslant x \leqslant L \tag{19}$$

$$\theta_{CO*}(x, 0) = \theta_{CO*}(x)^{ss}, \quad 0 \leqslant x \leqslant L \tag{20}$$

$$\theta_{O*}(x,0) = \theta_{O*}(x)^{ss}, \quad 0 \leqslant x \leqslant L \tag{21}$$

Boundary conditions at $x=0$ result from the oscillating feed at the inlet of the reactor. For CO

$$C_{f,1}(0, t) = \overline{C_{f,1}}[1 - B_1 \sin(2\pi ft)] \tag{22}$$

and for O_2

$$C_{f,2}(0, t) = \overline{C_{f,2}}\{1 - B_2 \sin[2\pi(ft + s)]\} \tag{23}$$

The phase angle $2\pi s$ that exists in practice in a car's catalytic converter amounts to about π radians, since the feed composition is cycled from lean to rich, *i.e.* from high O_2 and low CO to low O_2 and high CO. Table 2 shows the standard set of parameter values used in the calculations. The temperature-dependent parameters are given at 573 K.

The mathematical problem to be solved consists of the integration of a set of six partial differential equations, eqns. (13)–(17). To solve this set of equations, sixth-order orthogonal collocation [32] was applied in the x direction. At the inlet of the reactor, corresponding to the first collocation point x_1, the initial conditions of eqns. (22) and (23) hold. At each of the eight collocation points the

TABLE 2. Reactor parameter values used in this study

Parameter	Value	
a_{cat}	2.5×10^4	m$_{Pt}^2$ m$_R^{-3}$
a_v	2.4×10^3	m$_i^2$ m$_R^{-3}$
A_s	6.0×10^{-3}	m$_R^2$
d_b	1.0×10^{-3}	m$_R$
d_w	2.5×10^{-5}	m$_R$
k_f (573 K)	0.237	m$_f^3$ m$_i^{-2}$ s^{-1}
L	0.15	m$_R$
Sh	3.66	
ϵ	0.60	m$_f^3$ m$_R^{-3}$
ϵ_w	0.40	m$_f^3$ m$_w^{-3}$
ρ_f (573 K)	0.596	kg m$_f^{-3}$
G	0.0035, 0.035	kg s^{-1}
T	573, 623	K

six ordinary differential equations resulting from eqns. (13)–(17) have to be satisfied. The resulting set of 46 coupled ordinary non-linear differential equations have been integrated in time numerically using the routine D02EBF from the NAG library [33]. This routine integrates stiff ordinary differential equations using backward differentiation formulae with variable order and variable step size. Calculations were performed on a minisuper Alliant FX/2816 computer. A typical computation of one oscillation period required a CPU time of 5 s.

3. Results and discussion

The time average conversion during oscillatory feeding was studied relative to the steady state conversion as a function of frequency, amplitude, phase angle and CO/O_2 ratio. Calculations were performed at two different temperatures, 573 K and 623 K, and at three CO/O_2 ratios. The temperatures chosen are just below and just above the light-off temperature, which equals about 600 K and is defined here as the temperature at which 50% CO conversion is obtained for a stoichiometric feed. The stoichiometric equivalence ratio of the reactants is expressed relative to the stoichiometry of the global reaction and defined as

$$\phi = \frac{2\overline{C_f(O_2)}}{\overline{C_f(CO)}} \tag{24}$$

The time average CO and O_2 inlet concentrations during cycling corresponding to the chosen ratios ϕ are given in Table 3.

At frequencies above 1 Hz transient phenomena occurred before stable oscillations were obtained. All results reported here refer to situations beyond these initial transients.

As an example, typical for temperatures below the light-off temperature, Fig. 1 shows the oxygen bulk gas phase concentration as a function of both time and axial reactor coordinate. The corresponding oxygen surface coverages are presented in Fig. 2.

TABLE 3. Stoichiometric equivalent ratio ϕ and corresponding time average inlet composition. The balance is nitrogen

ϕ	$\overline{C_{f,CO}}$ (vol.%)	$\overline{C_{f,O_2}}$ (vol.%)
0.67	0.6	0.2
1.0	0.6	0.3
1.33	0.6	0.4
1.67	0.6	0.5
2.0	0.6	0.6

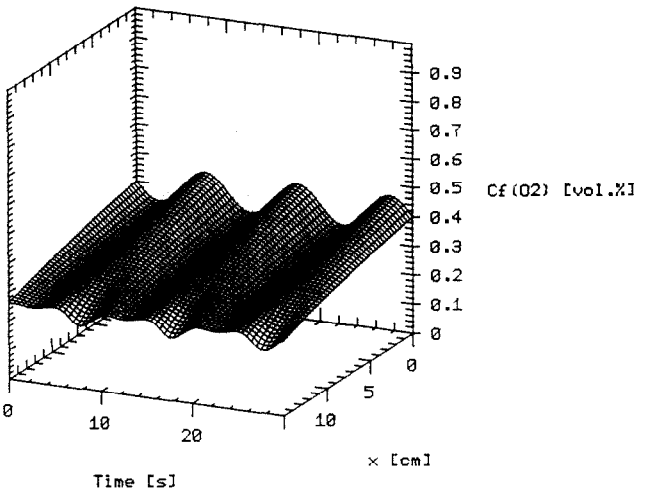

Fig. 1. O_2 bulk gas phase concentration as a function of axial reactor coordinate and time. $T=573$ K, $G=0.0035$ kg s^{-1}, $\phi=1.33$, $f=0.1$ Hz, $B=15\%$, phase angle π radians.

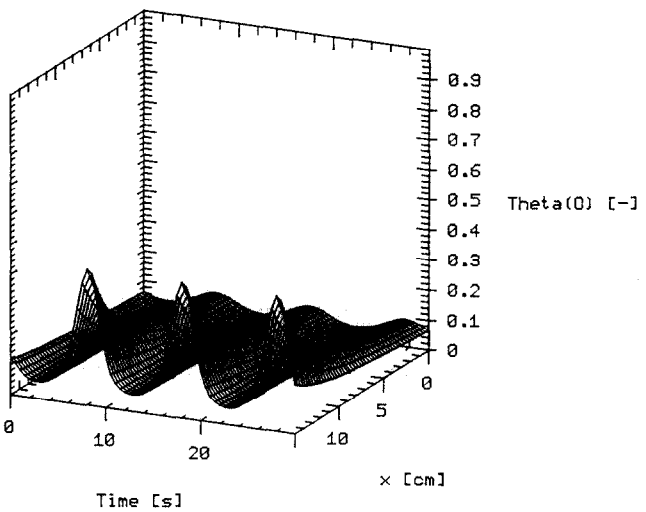

Fig. 2. O surface coverage as a function of axial reactor coordinate and time. $T=573$ K, $G=0.0035$ kg s^{-1}, $\phi=1.33$, $f=0.1$ Hz, $B=15\%$, phase angle π radians.

The concentrations inside the pores of the washcoat are not shown, but oscillate in phase with the gas phase concentrations at around 90% of the latter's values. The most striking feature in Fig. 1 is that maxima in the oxygen concentration at the reactor inlet turn into minima at the outlet. The maxima of the surface coverage of oxygen, however, become more pronounced near the reactor outlet. Notice the relatively low surface coverage of oxygen at this temperature. Figures 3 and 4 show the behaviour as a function of time for both CO and O_2 at the inlet as well as the outlet of the reactor. For CO the amplitudes of bulk gas concentration and surface coverage increase towards the reactor outlet. Remarkable is the strong periodic reduction in the CO

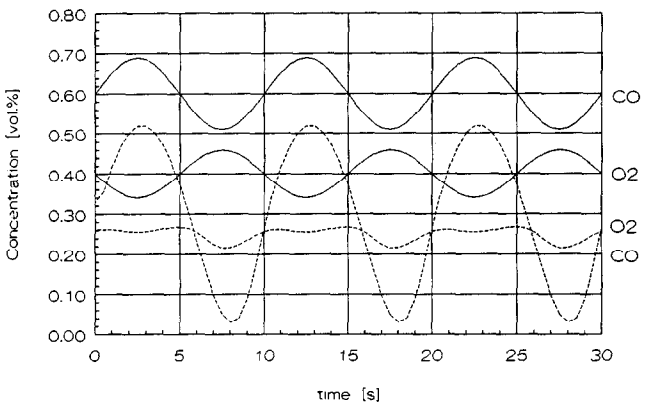

Fig. 3. Bulk gas phase concentrations of CO and O_2 *vs.* time at inlet (——) and outlet (----) of reactor. $T=573$ K, $G=0.0035$ kg s^{-1}, $\phi=1.33$, $f=0.1$ Hz, $B=15\%$, phase angle π radians.

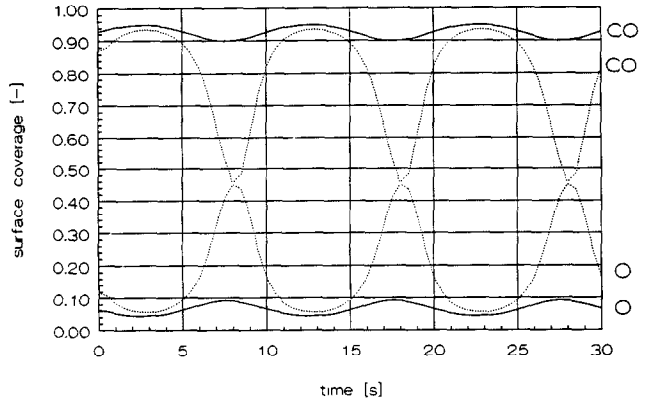

Fig. 4. Surface coverages of CO and O_2 *vs.* time at inlet (——) and outlet (----) of reactor. $T=573$ K, $G=0.0035$ kg s^{-1}, $\phi=1.33$, $f=0.1$ Hz, $B=15\%$, phase angle π radians.

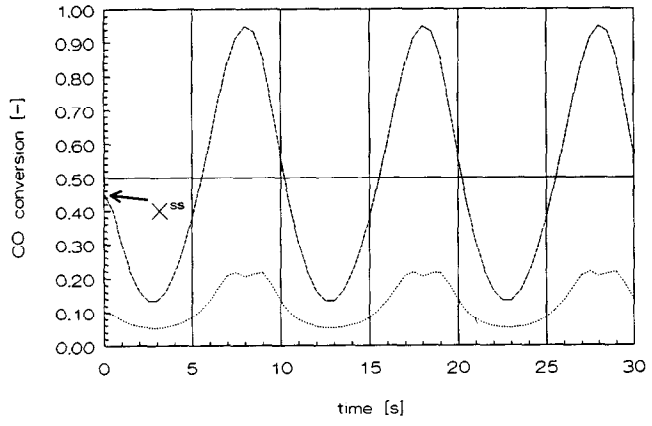

Fig. 5. Reaction rate (·····) in arbitrary units, actual CO conversion (----) and time average CO conversion (——). Note the steady state conversion at time $t=0$. $T=573$ K, $G=0.0035$ kg s^{-1}, $\phi=1.33$, $f=0.1$ Hz, $B=15\%$, phase angle π radians.

surface coverage near the reactor outlet. Figure 5 shows the reaction rate (in arbitrary units) and the actual CO conversion at the reactor outlet as well as the time average conversion, which is larger than the steady state conversion. This effect is more pronounced at high space times. The periodically enhanced reaction rate shows two close maxima around the minimum θ_{CO*} because of changing surface coverages of CO and O that oppose each other. In fact, the rate would be maximum when the surface coverage of both CO and O equals 0.5. The results are explained as follows.

In the steady state, corresponding to time $t=0$, the catalyst surface is almost completely covered with CO, resulting in a relatively low reaction rate due to CO inhibition of the adsorption of the second reactant. When the CO gas phase concentration increases owing to oscillation, even more CO adsorbs on the surface, which further decreases the reaction rate. In contrast, when the CO gas phase concentration decreases, free sites become available for O_2 adsorption and the rate increases accordingly. The fact that a CO decrease in the bulk gas phase is accompanied by an O_2 increase gives an extra enhancement of the rate and hence of the CO conversion. As a result of the positive feedback the amplitude of the CO oscillations is reinforced, whereas the negative feedback causes attenuation of the oxygen amplitude. At a certain position in the reactor this leads to a levelling-off of the oxygen oscillation. This occurs in Fig. 1 at a position around 10 cm. Owing to the continuing CO oscillation, an inversion occurs further downstream. The periodic reaction rate enhancement overcompensates the periodic decreases, leading to a positive effect on the time average conversion when compared with the steady state conversion (Fig. 5). This phenomenon is attributed to the non-linear character of the kinetics [34].

At a temperature above the light-off temperature the results are quite different. Figure 6 presents bulk gas phase concentrations at the inlet and outlet

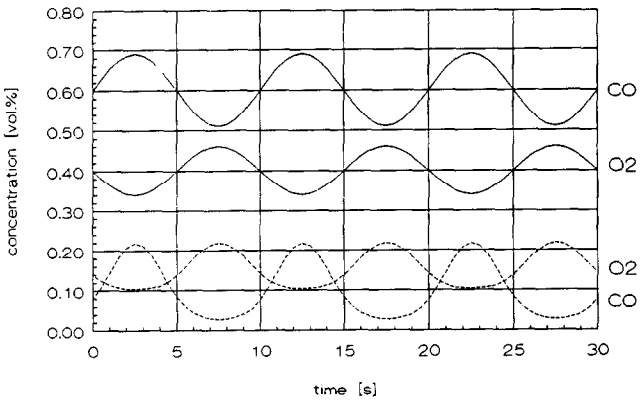

Fig. 6. Bulk gas phase concentrations of CO and O_2 *vs.* time at inlet (——) and outlet (----) of reactor. $T=623$ K, $G=0.035$ kg s^{-1}, $\phi=1.33$, $f=0.1$ Hz, $B=15\%$, phase angle π radians.

of the reactor for both CO and O_2. The corresponding surface coverages are shown in Fig. 7. The gas phase concentrations show only a small change in their oscillation amplitude between inlet and outlet. The CO surface coverage is relatively low at the reactor inlet and decreases further towards the outlet owing to lower gas phase concentrations. As a result more oxygen can be adsorbed, leading to higher oxygen coverage near the outlet. In the first half of the period the CO coverage increases with increasing gas phase concentration and vice versa in the second half. Oxygen shows a similar behaviour. Since a growing CO coverage is accompanied by a diminishing oxygen coverage, a rather constant reaction rate results during the first half of the period. However, when the CO coverage decreases further during the second half, θ_{0*} reaches its maximum and the reaction rate follows the decrease in θ_{CO*}. The net result is that the time average conversion of CO is less than the steady state conversion. The increase in amplitude of the CO coverage oscillation near the outlet may be caused by the fact that the amplitude of the CO gas phase oscillation is larger at the outlet when compared with the time average concentration. For oxygen a similar behaviour is found, but which is less pronounced because of an initial excess of oxygen ($\phi = 1.33$).

It is clear from the foregoing that the temperature has a large influence on the time average conversion and its deviation from the steady state conversion. This result corresponds with observations by Cho and West [13] in an experimental study of a cyclically operated Pt–Al_2O_3 catalyst bed for CO oxidation. An increase in the time average conversion is possible only if the surface is almost completely covered with CO at steady state. Therefore a positive effect of cycling is to be expected only below the light-off temperature, since such a situation only occurs at low temperatures. Above light-off the CO and O coverages are comparable at steady state and cycling of the feed does not improve the performance.

As such this work provides a theoretical basis for adjusting the settings of the microprocessor controller in a real exhaust gas converter, since the experimental work of Cho [12] has shown that this behaviour is similar for other exhaust gas reactions.

The influences of frequency, amplitude, phase angle and CO/O_2 ratio were studied in order to assess the regions in which an increase or decrease in time average conversion during cycling of the feed occurs.

Figure 8 shows the increase in time average conversion relative to the steady state conversion at 573 K as a function of cycle period and amplitude at a phase angle of π radians and $\phi = 1$. At periods higher than 10 s no further increase in time average conversion relative to the steady state conversion occurs; the relative increase stabilizes close to 10%. At periods lower than 0.1 s the relative increase in CO conversion is very small, since high frequency oscillations cannot be followed. The increase in time average conversion increases strongly with amplitude. Apparently changes in surface coverage, which underlie the improved time average conversion, are reinforced by larger amplitudes.

Figure 9 shows the relative increase in time average conversion at 573 K as a function of cycle period and phase angle with an amplitude of 15%. A maximum in the relative increase occurs at a phase angle of π radians, *i.e.* when CO and O_2 oscillate exactly in counterphase, as is the case in automotive converter practice.

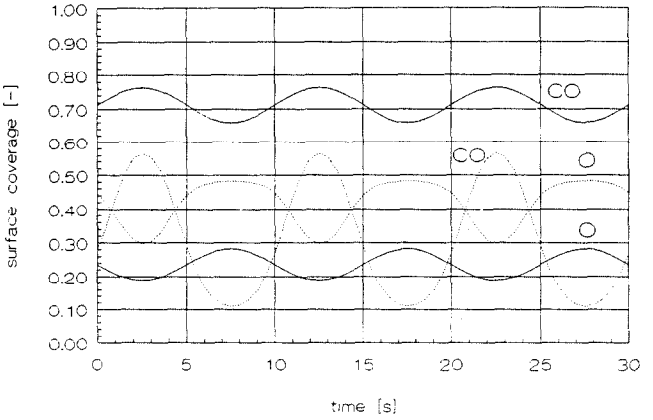

Fig. 7. Surface coverages of CO and O_2 *vs.* time at inlet (——) and outlet (----) of reactor. $T = 623$ K, $G = 0.035$ kg s^{-1}, $\phi = 1.33$, $f = 0.1$ Hz, $B = 15\%$, phase angle π radians.

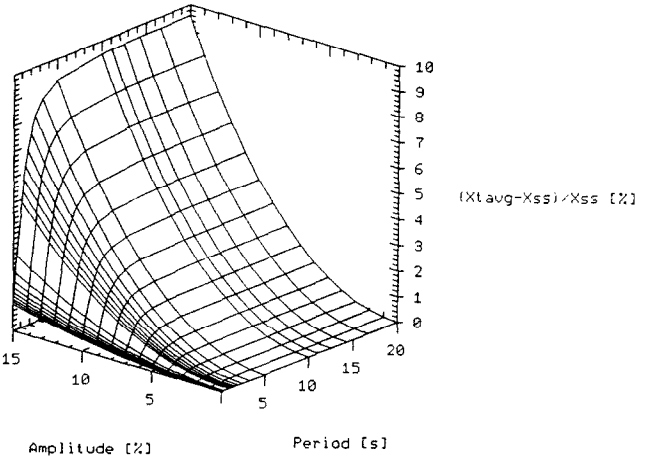

Fig. 8. Increase in time average CO conversion relative to steady state conversion as a function of cycle period and amplitude. $T = 573$ K, $G = 0.0035$ kg s^{-1}, $\phi = 1$, phase angle π radians.

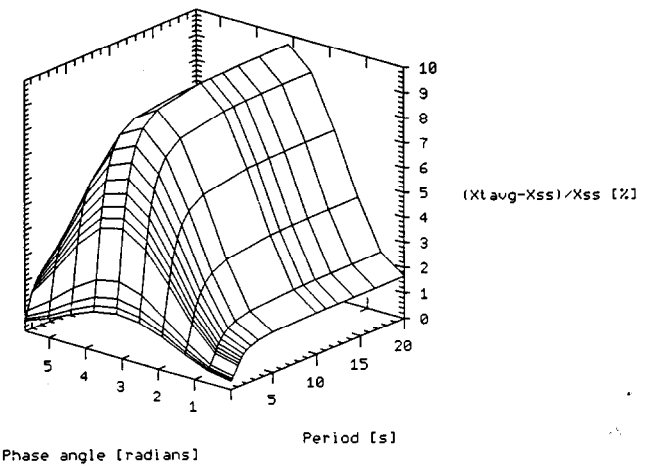

Fig. 9. Increase in time average CO conversion relative to steady state conversion as a function of cycle period and phase angle. $T=573$ K, $G=0.0035$ kg s^{-1}, $\phi=1$, $B=15\%$.

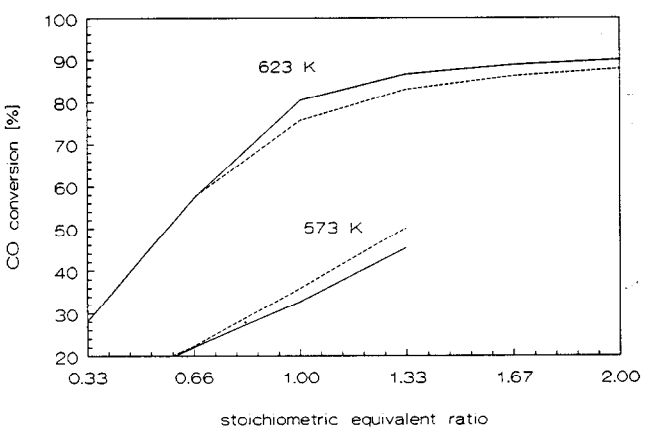

Fig. 10. CO conversion *vs.* stoichiometric equivalent ratio ϕ for steady state (——) and periodic (----) operation. Upper curves: $T=623$ K, $G=0.035$ kg s^{-1}. Lower curves: $T=573$ K, $G=0.0035$ kg s^{-1}. Common conditions: $f=0.1$ Hz, $B=15\%$, phase angle π radians.

Simulations were also performed with different ϕ values. Figure 10 compares the cycling and steady state behaviour for temperatures above and below light-off. The increase in the time average CO conversion compared with the steady state conversion becomes more pronounced below light-off with increasing ϕ. Above light-off the effect of cycling also becomes more pronounced, but negative, with increasing ϕ.

4. Conclusions

The time average CO conversion during oscillatory feeding predicted by the present model is higher relative to the steady state conversion at temperatures (573 K) below the reaction light-off temperature, whereas this trend reverses at temperatures (623 K) above the light-off temperature. Induced feed oscillations improve the performance below light-off, whereas above light-off the air–fuel ratio should be kept as near as possible to the stoichiometric ratio. The change in CO conversion by cycling of the feed results from strongly changed surface coverages during cycling compared with steady state surface coverages.

The maximum of $\pm 10\%$ increase in time average CO conversion occurs for frequencies below 0.1 Hz and a phase angle of π radians between CO and O_2, *i.e.* counterphase oscillation. The size of the effect increases strongly with amplitude. The effect is also enhanced by an initial excess of oxygen.

Clearly there is an incentive to set the frequency of the converter feed composition rather than to accept it as a result of a control loop which is designed solely to keep the feed composition close to the stoichiometric point.

References

1 J. Wei, Catalysis for motor vehicle emissions, *Adv. Catal.*, *24* (1975) 57–129.
2 K.C. Taylor, in J.R. Anderson and M. Boudart (eds.), *Catalysis Science and Technology*, Vol. 5, Springer, Berlin, 1984, p. 119.
3 S. Irandoust and B. Andersson, *Catal. Rev. – Sci. Eng.*, *30* (3) (1988) 341–392.
4 J.C. Schlatter, R.M. Sinkevitch and P.J. Mitchell, *Ind. Eng. Chem. Prod. Res. Develop.*, *22* (1983) 51–56.
5 M.B. Cutlip, *AIChE J.*, *25* (3) (1979) 502–508.
6 G. Vaporciyan, A. Annapragada and E. Gulari, *Chem. Eng. Sci.*, *43* (11) (1988) 2957–2966.
7 X. Zhou and E. Gulari, *Chem. Eng. Sci.*, *41* (4) (1986) 883–890.
8 X. Zhou, Y. Barshad and E. Gulari, *Chem. Eng. Sci.*, *41* (5) (1986) 1277–1284.
9 R.C. Graham and D.T. Lynch, *AIChE J.*, *36* (12) (1990) 1796–1806.
10 R.K. Herz, J.B. Kiela and J.A. Sell, *Ind. Eng. Chem. Prod. Res. Develop.*, *22* (1983) 387–396.
11 K.C. Taylor and R.M. Sinkevitch, *Ind. Eng. Chem. Prod. Res. Develop.*, *22* (1983) 45–51.
12 B.K. Cho, *Ind. Eng. Chem. Res.*, *27* (1988) 30–36.
13 B.K. Cho and L.A. West, *Ind. Eng. Chem. Fund.*, *25* (1986) 158–164.
14 J.A. Moulijn and F. Kapteijn, *Chem. Mag.*, (1989) 499–501.
15 B.K. Cho, *Ind. Eng. Chem. Fund.*, *22* (1983) 410–420.
16 W.R.C. Graham and D.T. Lynch, *AIChE J.*, *36* (12) (1990) 1796–1806.
17 S.E. Voltz, C.R. Morgan, D. Liedermann and S.M. Jacob, *Ind. Eng. Chem. Prod. Res. Develop.*, *12* (1973) 294–301.
18 J.C. Schlatter and T.S. Chou, Measuring oxidation rates in a recycle reactor, *AIChE 71st Ann. Meet., Miami Beach, FI, November 1978.*
19 R.K. Herz and S.P. Marin, *J. Catal.*, *65* (1980) 281–296.
20 A. Golchet and J.M. White, *J. Catal.*, *53* (1978) 266–279.

21 L.C. Young and B.A. Finlayson, *AIChE J.*, *22* (2) (1976) 331–343.
22 L.C. Young and B.A. Finlayson, *AIChE J.*, *22* (2) (1976) 343–353.
23 J. Votruba, J. Sinkule, V. Hlavacek and J. Skrivanek, *Chem. Eng. Sci.*, *30* (1975) 117–123.
24 J.W. Kress, N.C. Otto, M. Bettman, J.B. Wang and A. Varma, *AIChE Symp. Ser.*, *76* (1980) 202–211.
25 J.S. Howitt and T.C. Sekella, *SAE Paper 740244*, 1974.
26 K. Zygourakis, *Chem. Eng. Sci.*, *44* (9) (1989) 2075–2086.
27 D.F. Sherony and C.W. Solbrig, *Int. J. Heat Mass Transfer*, *13* (1970) 145–159.
28 R.K. Shah and A.L. London, *Advances in Heat Transfer*, Suppl. 1, *Laminar Flow Forced Convection in Ducts: A Source Book for Compact Heat Exchanger Analytical Data*, Academic, London, 1978.
29 R.C. Reid, J.M. Prausnitz and B.E. Poling, *The Properties of Gases and Liquids*, McGraw-Hill, New York, 4th edn., 1987, p. 587.
30 P.B. Weisz and C.D. Prater, *Adv. Catal.*, *6* (1954) 143.
31 A.N.R. Bos and K.R. Westerterp, *Chem. Eng. Commun.*, *99* (1991) 139–153.
32 B.A. Finlayson, in R. Bellman (ed.), *Mathematics in Science and Engineering*, Vol. 87, Academic, New York, 1972.
33 *Numerical Algorithm Group Routine D02EBF, NP 1490/13*, 1991.
34 Yu.Sh. Matros, *Catalytic Processes Under Steady State Conditions*, Elsevier, Amsterdam, 1989.

Appendix A: Nomenclature

a_{cat} catalytic surface area per unit reactor volume ($m_{Pt}^2\ m_R^{-3}$)
a_v geometric surface area per unit reactor volume ($m_i^2\ m_R^{-3}$)
A pre-exponential factor
A_s cross-sectional area of monolith (m_F^2)
B amplitude as a percentage of $\overline{C_{f,i}}$ (%)
c_{pf} heat capacity of fluid (J kg^{-1} K^{-1})
C concentration (mol m_f^{-3})
d_b internal diameter of channel (m_R)
d_w thickness of washcoat (m_R)
D diffusion coefficient ($m_f^3\ m^{-1}\ s^{-1}$)
E_A activation energy (kJ mol^{-1})
f frequency (Hz)
G mass flow (kg s^{-1})
Gr Graetz number, $(Re\ Pr)^{-1}\ L/d_b$
$k_{a,i}$ adsorption coefficient for species i ($m_f^3\ mol^{-1}\ s^{-1}$)
$k_{d,i}$ desorption coefficient for species i (s^{-1})
k_f mass transfer coefficient ($m_f^3\ m_i^{-2}\ s^{-1}$)
k_r reaction rate coefficient (s^{-1})
L reactor length (m_R)
L_t moles of Pt per unit catalytic surface area (mol m_{Pt}^{-2})
M molar mass (kg mol^{-1})
Pr Prandtl number, $\mu c_{pf}/\lambda_f$
r reaction rate (mol $m_{Pt}^{-2}\ s^{-1}$)
R gas constant (kJ mol^{-1} K^{-1})
Re Reynolds number, Gd_b/μ
s cycle split, phase angle
S_i sticking coefficient for component i
Sh Sherwood number, $k_f d_b/D$
t time (s)
T temperature (K)
x axial coordinate (m_R)
X conversion

Greek letters
ϵ void fraction of monolith ($m_f^3\ m_R^{-3}$)
ϵ_w washcoat porosity ($m_f^3\ m_w^{-3}$)
θ surface coverage (mol mol_{Pt}^{-1})
λ_f thermal conductivity of fluid (W m^{-1} K^{-1})
μ dynamic viscosity of fluid (kg m^{-1} s^{-1})
ρ_f gas density (kg m_f^{-3})
ϕ stoichiometric equivalence ratio
ϕ_m^{sup} superficial mass flow (kg $m_R^{-2}\ s^{-1}$)

Subscripts
a adsorption
cat catalyst
d desorption
f bulk gas phase
i interface
i referring to reactant i
r reaction
R reactor
s pores in washcoat
w washcoat
1 referring to CO
2 referring to O_2

Superscripts
in inlet
ss steady state
tavg time average